

RSC Advances



This is an *Accepted Manuscript*, which has been through the Royal Society of Chemistry peer review process and has been accepted for publication.

Accepted Manuscripts are published online shortly after acceptance, before technical editing, formatting and proof reading. Using this free service, authors can make their results available to the community, in citable form, before we publish the edited article. This *Accepted Manuscript* will be replaced by the edited, formatted and paginated article as soon as this is available.

You can find more information about *Accepted Manuscripts* in the [Information for Authors](#).

Please note that technical editing may introduce minor changes to the text and/or graphics, which may alter content. The journal's standard [Terms & Conditions](#) and the [Ethical guidelines](#) still apply. In no event shall the Royal Society of Chemistry be held responsible for any errors or omissions in this *Accepted Manuscript* or any consequences arising from the use of any information it contains.

Novel nanostructured star-shaped polyaniline derivatives and their electrospun nanofibers with gelatin

Bakhshali Massoumi¹, Nazila Aali¹, and Mehdi Jaymand^{2,*}

1. Department of Chemistry, Payame Noor University, P.O. BOX: 19395-3697 Tehran, Islamic Republic of Iran.
2. Research Center for Pharmaceutical Nanotechnology, Tabriz University of Medical Sciences, P.O. Box: 51656-65811, Tabriz, Islamic Republic of Iran.

* Correspondence to: Mehdi Jaymand, Research Center for Pharmaceutical Nanotechnology, Tabriz University of Medical Sciences, Tabriz, Iran
Tel: +98-41-33367914; Fax: +98-41-33367929
Postal address: Tabriz-5165665811-Iran
E-mail addresses: m_jaymand@yahoo.com; m.jaymand@gmail.com; jaymandm@tbzmed.ac.ir

Abstract

The aim of this study is the synthesis, characterization, and investigation of some physicochemical properties of the star-shaped polyaniline and polyanisidine. The star-shaped conductive polymers were synthesized chemically and electrochemically *via* a “core-first” method from tannic acid. The chemical structures of all samples as representatives were characterized by means of Fourier transform infrared (FTIR), and ^1H nuclear magnetic resonance (NMR) spectroscopies. The electroactivity behaviors of the synthesized samples were verified under cyclic voltammetric conditions, and their conductivities were determined using the four-probe technique. According to results, the synthesized star-shaped polymers showed higher electrical conductivity and electroactivity than those of the corresponding homo-polymers in both chemical and electrochemical approaches. These results originated from the spherical, three-dimensional, and nanostructure morphologies of the star-shaped polymers, which allows sufficient overlapping of π -orbitals. The solutions of the chemically synthesized star-shaped conducting polymers, and gelatin were electrospun to produce uniform, conductive, and biocompatible nanofibers.

Keywords: Polyaniline, Star-shaped, Tannic acid, Gelatin, Electrospun, Nanofibers

1. Introduction

Since the discovery of electrically conducting polymers (ECPs) in 1977, the polymerization methods, chemical modification of these polymers, and their application fields have progressed significantly [1-6]. Among them, aromatic polymers such as polypyrrole (PPy), polythiophene (PTh), and polyaniline (PANI) are particular of interest, in part due to their unique physicochemical properties [7-12]. In this respect, the PANI has been intensively explored both theoretically, and experimentally, and considered as one of the most promising material due to its unique physicochemical properties such as excellent redox reversibility, good thermal and environmental stability, controllable electrical conductivity, high energy density, ease of synthesis, and low cost [11, 13-16]. In addition, the PANI has great potentials in many areas such as shielding of equipments from electromagnetic interference [17], anticorrosive applications [18], waste water treatment [19], biomedical sciences [20], rechargeable batteries [21], electrochromic display material [22], photovoltaic devices [23], organic light emitting diodes (OLEDs) [24], electrorheological (ER) material [25], electrical memory performance [26], bio and chemical sensors [27], and many more.

It is an unquestionable fact that, the last decade has witnessed the development of novel multifunctional materials in broad range of practical and technological applications. The emergence of nanotechnology has provided exciting new possibilities for development of new multifunctional materials with improved physicochemical properties in various multidisciplinary fields such as biology, physics, chemistry, engineering, *etc* [28-33]. Depending on the synthetic conditions the PANI has been isolated in different morphologies such as fibers, wires, microwebs, hemispheres, and other morphologies

[34, 35]. It should be pointed out that the nanostructured PANI offers superior electrochemical properties; however, the conventional chemical oxidative polymerization approach yields granular PANI [27, 36, 37]. Various synthetic routes, such as microemulsion [38], interfacial polymerization [39], template synthesis [40], self-assembly [41], and electrochemical polymerization [42], have been adopted to synthesize nanostructured PANI.

In this respect, star-shaped PANIs have stimulated great interest on the basis of their unique three-dimensional shape and physicochemical properties. Star-shaped polymers, which are composed of multiple polymer chains emanating from junction points, have attracted a great deal of interest over the past decade, in part due to their ability to pack in three-dimensions [37, 43]. The conductivity in PANI depends on both intramolecular and intermolecular charge transport. The spherical and three-dimensional structure of the star-shaped PANI gives it the conductive characteristics that are better than the linear counterpart. In addition, this property is originated from the stereochemistry of the star-shaped PANI chains, which allows sufficient overlap of π -orbitals [44, 45]. For instance, Xiong *et al.* reported the synthesis and characterization of star-like PANI doped with poly(4-styrene sulfonic acid) (PSS), and dodecylbenzene sulphonic acid (DBSA) from octa(aminophenyl) silsesquioxane (OAPS) as core. According to the results, they concluded that the synthesized star-like polyanilines possess much greater thermodynamic penetrability in solution, as detected using static and dynamic light scattering in comparison with homo-polyaniline [43].

It deserves to be mentioned here, that a relatively novel achievement with PANI is its tissue engineering performance, in part due to its good electrical conductivity, reversible

oxidation, redox stability, biocompatibility, and hydrophobicity (40–70° water contact angle promotes cell adhesion). It should be pointed out that the PANI in purified form exhibits relatively good biocompatibility, which is further enhanced by blending with biodegradable polymers such as poly(ethylene glycol), chitosan, gelatin, and many more [37, 46-50]. For this purpose, electrospinning is proposed as an efficient and versatile strategy to prepare biocompatible conductive nanofibers. This technique has attracted great interest in the fabrication of scaffolds for repair and regeneration of human tissues, in part due to high porosity, ultra-thin continuous fibers, high surface-to-volume ratio, and adjustable pore size distribution [47, 51, 52].

In this work, we explore the synthesis, characterization, and some physicochemical properties of the star-shaped polyaniline derivatives with tannic acid core. First, the tannic acid was functionalized with *p*-anthranilic acid in the presence of *p*-toluenesulfonic acid (*p*-TSA) as the dehydrating agent to afford a phenylamine-functionalized tannic acid macromonomer (PhATAM). The synthesized PhATAM subsequently employed in both chemical and electrochemical oxidation copolymerizations with aniline and anisidine (ANIS) monomers to produce star-shaped conducting polymers. The solutions of the chemically synthesized star-shaped PANI and PANIS were electrospun with gelatin solution to produce uniform, conductive, and biocompatible nanofibers.

2. Experimental

2.1. Materials

The monomers (aniline and anisidine) were purchased from Merck (Darmstadt, Germany), and were distilled twice under reduced pressure before use. Tannic acid (TA), and gelatin (bovine skin, type B powder) were purchased from Sigma-Aldrich (USA),

and were used as received. Toluene (Merck) was dried by refluxing over sodium, and distilled under argon prior to use. Ammonium peroxydisulfate (APS) from Merck was re-crystallized at room temperature from ethanol–water. Camphorsulfonic acid (CSA), *p*-toluenesulfonic acid (*p*-TSA), and *p*-anthranilic acid were purchased from Merck, and were used as received. All other reagents were purchased from Merck, and purified according to standard methods.

2.2. Synthesis of PhATAM

The PhATAM was synthesized by the esterification of tannic acid with *p*-anthranilic acid in the presence of *p*-TSA as a catalyst. Briefly, a 100 ml three-neck round-bottom flask equipped with a dean-stark trap, gas inlet/outlet, and a magnetic stirrer, was charged with tannic acid (3g, 1.76 mmol), *p*-anthranilic acid (6.25 g, 45 mmol), and anhydrous toluene (80 ml). A catalytic amount of *p*-TSA (0.1 g, 0.55 mmol) as the dehydrating agent was added to the flask, and the reaction mixture was de-aerated by bubbling highly pure argon for 10 minutes. Thereafter, the flask placed in a silicon oil bath at 110 ± 3 °C, and the reaction mixture was stirred for about 24 hours under argon atmosphere. The water of the reaction was removed as an azeotrope until no more water was formed. It could mean that the reaction had gone to completion. Then, the reaction flask was cooled to room temperature by ice water bath, the crud product was filtered, and dried in vacuum at room temperature. The crud product was purified by re-crystallization from acetonitrile for three times (Scheme 1).

(Scheme 1)

2.3. Synthesis of star-shaped PANI, and PANIS *via* chemical oxidation polymerization

A 250 ml round-bottom flask was charged with PhATAM (1 g), DMSO (30 ml), deionized water (10), aniline monomer (3 ml, 32 mmol), and CSA (15 g, 65 mmol). The reaction mixture was stirred vigorously for about 1 hour to obtain homogeneous solution, and then temperature was reduced to 0 °C. In a separate container, 8 g (35 mmol) of APS was dissolved in 40 ml deionized water, and was slowly added to the reaction mixture at a rate of 5 ml min⁻¹. The reaction mixture was stirred for about 24 hours at 0 °C, and then the reaction was terminated by pouring the content of the flask into a large amount of methanol. The resultant powder was filtered, and dried in vacuum at room temperature (Scheme 2). The star-shaped PANIS was synthesized by the same method, through the addition of 3.6 ml (32 mmol) of anisidine monomer instead aniline monomer. In addition, the homo-PANI, and homo-PANIS were synthesized by the same method in the absence of the PhATAM macromonomer.

(Scheme 2)

2.4. Synthesis of star-shaped PANI, and PANIS *via* electrochemical oxidation polymerization method

The star-shaped PANI, and PANIS were synthesized by applying sequential linear potential sweeps with a scan rate of 25 mV s⁻¹ between -0.2 and +1.0 V *versus* silver (Ag)/silver chloride (AgCl) electrode. For this purpose, a 3% (w/v) solution of the PhATAM macromonomer was prepared in tetrahydrofuran (THF), and both sides of working electrode (glassy carbon electrode) were coated with PhATAM by drop-coating.

The samples were synthesized through 10 cycles in the supporting electrolyte. The electrolyte solution consists of 0.1 mol l^{-1} aniline or anisidine, and 1.0 mol l^{-1} CSA.

2.5. Electrospinning of the chemically synthesized star-shaped PANI, and PANIS with gelatin

The nanofibers of chemically synthesized star-shaped PANI/gelatin, and star-shaped PANIS/gelatin were prepared by an electrospinning apparatus was equipped with a high voltage power supply (Gamma High Voltage Research E8-50P, Ormond Beach, FL, USA). Immediately before electrospinning, CSA-doped star-shaped PANI (0.2 g) was dissolved in DMSO (10 ml) with vigorous stirring at room temperature for about 3 hours, followed by filtering through a regular qualitative filter paper (Whatman). In a separate container, 0.3 g of gelatin was dissolved in DMSO (10 ml) with stirring at room temperature for about 1 hour. Thus, the concentrations of the CSA-doped star-shaped PANI, and gelatin solutions were 2 and 3% w/v. Samples for electrospinning were then prepared by mixing two solutions at volume ratios of CSA-doped star-shaped PANI to gelatin at 30:70. The polymers solutions were added to a 10 ml syringe with a 23G hypodermic needle used as the nozzle. The flow rate of the polymer solution was controlled with a precision pump (JZB 1800D double channel syringe pump, China) to maintain a steady flow from the capillary outlet. The solution was injected at the rate of 0.5 ml h^{-1} , and the applied voltage was set to 20 kV. The static collector was wrapped with aluminum foil, and located at a fixed working distance of 15 cm from the needle tip. After fiber deposition, the fiber mats was dried in vacuum at room temperature. The star-shaped PANIS/gelatin nanofibers were prepared in the same condition.

2.6. Characterization

Fourier transform infrared (FTIR) spectra of the samples were recorded on a Shimadzu 8101M FTIR (Shimadzu, Kyoto, Japan) between the frequency range of 4000 to 400 cm^{-1} , with an attenuated total reflection facility. The instrumental resolution was set at 4 cm^{-1} . The samples were prepared by grinding the dry powders with potassium bromide (KBr), and compressing the mixture into disks. The spectra were recorded at room temperature. The ^1H nuclear magnetic resonance (NMR) spectra were recorded at 25 $^\circ\text{C}$ using an FT-NMR (400 MHz) Bruker spectrometer (Bruker, Ettlingen, Germany). The sample for NMR spectroscopy was prepared by dissolving about 10 mg of samples in 1 ml of deuterated dimethyl sulfoxide ($\text{DMSO-}d_6$), and chemical shifts were reported in ppm units with tetramethylsilane as internal standard. The field emission scanning electron microscope (FE-SEM) type 1430 VP (LEO Electron Microscopy Ltd, Cambridge, UK) was applied to determine the morphologies of the synthesized samples. Ultraviolet-visible (UV-vis) absorption spectra of the samples were measured using a Shimadzu 1601 PC UV-vis spectrophotometer (Shimadzu, Kyoto, Japan) in the wavelength range of 300–1000 nm. Electrochemical experiments were conducted using Auto-Lab PGSTA T302N. The electrochemical cell contained five openings: three of them were used for the electrodes (working, counter, and reference), and two for argon bubbling in the solutions during all experiments. The conductivity of the synthesized samples was determined using the four-probe technique (Azar Electrode, Urmia, Iran) at room temperature. The wettability of the electrospun nanofibers were investigated by drop water contact angle measurement using an OCA 20 Plus contact angle meter system

(DataPhysics Instruments GmbH, Filderstadt, Germany). The droplet size was 0.5 μl , and at least five samples were used for each test.

3. Results and discussion

In recent years, more and more research efforts have been devoted on the design, and development of new organic materials for both optical and electronic applications. Considerable advances and promising results have been obtained, in the academic and industrial communities. Nevertheless, this field is still growing and many issues remain to be answered. In this respect, intrinsically conductive polymers (especially polyaniline, and its derivatives) are particular of interest.

3.1. Characterization of PhATAM

The FTIR spectra of the tannic acid, and PhATAM are shown in Figure 1. The FTIR spectrum of the tannic acid shows the characteristic absorption bands due to the aromatic C=C stretching vibrations at 1607 and 1447 cm^{-1} , the broad band centered at 3378 cm^{-1} is assigned to the stretching vibrations of hydroxyl groups, the stretching vibrations of carbonyl groups at 1706 cm^{-1} , $\gamma(\text{C-H})$ in the aromatic ring at 865 and 752 cm^{-1} , C-O stretching vibrations at 1312 cm^{-1} , C-O-C stretching vibration at 1118 cm^{-1} , and weak aromatic overtone and combination bands in the 1900 to 1750 cm^{-1} region. It should be pointed out that, the aliphatic and aromatic C-H stretching vibrations are overlapped with the very strong band of the hydroxyl groups (2800-3700 cm^{-1}). In comparison with the FTIR spectrum of the tannic acid, the most significant changes in the FTIR spectrum of the PhATAM are the appearance of $-\text{NH}_2$ stretching vibrations at 3360 and 3223 cm^{-1} , and the stretching vibrations of aliphatic and aromatic C-H at 3050 to 2800 cm^{-1} region. In addition, as seen in this spectrum the intensity of the hydroxyl stretching vibration is

decreased significantly (3458 cm^{-1}). This is verified that most of the hydroxyl groups were reacted with *p*-anthranilic acid.

(Figure 1)

The synthesized PhATAM was further characterized by means of ^1H NMR spectroscopy. The ^1H NMR spectra of the TA, and PhATAM are shown in Figure 2. The aliphatic protons of glucose core in the tannic acid are appeared at 3.00-4.00 ppm. It is important to note that the resonances at about 6.35–6.50 ppm are assigned to the anomeric proton of the glucose core. The chemical shifts at 6.70-7.70 and 8.80-10.20 ppm are related to the aromatic protons, and hydroxyl groups of the TA, respectively. The chemical shifts at 2.50 and 3.33 ppm are assigned to the H_2O and dimethyl sulfoxide (as impurities in NMR solvent), respectively.

The ^1H NMR spectrum of the PhATAM shows the chemical shifts of aliphatic and aromatic protons of the TA core at 3.35 and 6.80 ppm, respectively. The chemical shift at 5.90 ppm is related to the $-\text{NH}_2$ groups of *p*-aminobenzoate. In addition, the aromatic protons of the *p*-aminobenzoate are appeared at 7.40 ppm.

(Figure 2)

3.2. Synthesis of homo and star-shaped PANI and PANIS

The chemically synthesized star-shaped PANI and PANIS, and their corresponding homo-polymers were characterized by means of FTIR spectroscopy as shown in Figures 3 and 4. The FTIR spectrum of the homo-PANI shows the characteristic absorption bands due to the stretching vibrations of aromatic C–H ($3050\text{--}2900\text{ cm}^{-1}$), $\gamma(\text{C–H})$ in the aromatic ring at 741 cm^{-1} , the N–H stretching vibration at 3524 cm^{-1} , stretching vibration of the C=C in the benzenoid units at 1502 cm^{-1} , $\text{C}_{\text{aromatic}}\text{--N}$ stretching vibration at 1301

cm^{-1} , and weak aromatic overtone and combination bands in the 1900 to 1650 cm^{-1} region. The FTIR spectrum of the star-shaped PANI shows similar bands with minor differences. The most significant changes can be listed as: a strong band at 1706 cm^{-1} (related to the carbonyl groups of tannic acid core, C–O–C stretching vibration at 1284 cm^{-1} , and the band at 3221 cm^{-1} may be attributed to the hydroxyl groups of the tannic acid, which are not reacted with the *p*-antheranilic acid.

(Figure 3)

The FTIR spectrum of the star-shaped PANIS and homo-PANIS are shown in Figure 4. As seen in this figure, the FTIR spectrum of the homo-PANIS shows the characteristic absorption bands due to the stretching vibrations of C–H at 3050–2900 cm^{-1} , $\gamma(\text{C–H})$ in the aromatic ring at 741 and 820 cm^{-1} , the N–H stretching vibration at 3537 cm^{-1} , stretching vibration of the C=C in the benzenoid units at 1493 cm^{-1} , C_{aromatic}–N stretching vibration at 1293 cm^{-1} , weak aromatic overtone and combination bands in the 1900 to 1650 cm^{-1} region, and C–O–C stretching at 1116 cm^{-1} . As mentioned in the case of star-shaped PANI, the star-shaped PANIS shows similar bands with minor differences. The most significant change is a relatively strong band at 1706 cm^{-1} , which can be assigned to the carbonyl groups of the tannic acid core. In addition, the broad band centered at 3100 cm^{-1} may be assigned to the hydroxyl groups of tannic acid, which are not reacted with the *p*-antheranilic acid.

(Figure 4)

3.3. Morphology study

As shown in Figure 5, the surface morphology of the chemically synthesized homo and star-shaped polymers were observed by means of FE-SEM. As seen in Figure 5a and b,

both homo-PANI, and homo-PANIS shows the compressed microstructure. In contrast, the star-shaped polyaniline and polyanisidine (Figure 5c and d) exhibits nanostructure, and porous morphology with an average diameter of 100 ± 20 nm. The difference morphologies of the star-shaped polymers in comparison with homo-polymers may be originated from the controlled growth of PANI and PANIS chains from PhATAM macromonomer.

(Figure 5)

3.4. Electroactivity behaviors of the chemically synthesized homo and star-shaped PANI and PANIS

As shown in Figure 6, the effect of the potential scanning rate (V) on the peak currents for the chemically synthesized homo and star-shaped PANI and PANIS were investigated under cyclic voltammetric (CV) conditions in the range of 10 to 90 mV s^{-1} scan rate, in the aqueous solution of CSA (1 mol l^{-1}) between -0.20 and +1.00 V. All potentials are given *versus* the reference (Ag/AgCl) electrode. The polymer film was prepared on glassy carbon (GC) microelectrode by casting the polymeric solution of samples, which prepared as follows. The same amounts of the samples were dissolved in THF followed by ultrasonic treatment for 10 minutes.

Typical cyclic voltammograms (CVs) of the homo-PANI film are shown in Figure 6a. As seen the CVs of the homo-PANI shows two anodic peaks at approximately 0.43 and 0.68 V *versus* the reference electrode. Moreover, as can be seen the anodic peaks shifts in the direction of positive potential with increasing scan rate, which indicates the electrochemical doping/dedoping of the casted polymer film was chemically reversible. The CVs of the star-shaped PANI film (Figure 6b) exhibits two typical redox couples

with anodic peaks at approximately 0.32 and 0.48 V *versus* the Ag/AgCl electrode. In addition, similar to CVs of the homo-PANI in CVs of the star-shaped PANI anodic peaks shifts in the direction of positive potential with increasing scan rate.

The CVs of the homo-PANIS are shown in Figure 6c. The CVs of this sample shows two anodic peaks at approximately 0.37 and 0.61 V *versus* the reference electrode. In similar the CVS of the star-shaped PANIS (Figure 6d) exhibits two typical redox couples with anodic peaks at approximately 0.38 and 0.52 V *versus* the reference electrode. It is important to note that in both homo and star-shaped PANIS the anodic peaks shifts in the direction of positive potential with increasing scan rate, which indicates the electrochemical oxidation/reduction of the casted polymer films were chemically reversible.

(Figure 6)

For additional evidence on the redox activity of the chemically synthesized samples the relationship between the peaks current sizes *versus* scan rates were determined. The linear relationships between the current and scan rate in the range of 10 to 90 mV s⁻¹ for these samples are shown in Figure 7. This linear relationship is typical of redox-active polymers attached to the working electrode (GCE), and also exemplifies the stability of the synthesized samples toward doping/dedoping. In the end of this section, it should be pointed out that the chemically synthesized star-shaped PANI (S-PANI), and PANIS (S-PANIS) showed higher electroactivity than those of the corresponding homo-polymers (H-PANI and H-PANIS), in part due to their three-dimensional structure, which allows sufficient overlap of π -orbitals. In additional, both star-shaped and homo-PANI showed higher electroactivity than those of the corresponding polyanisidines. This may be

resulted from reducing of conjugated length by methoxy group in the case of the polyanisidines.

(Figure 7)

3.5. Synthesis of homo and star-shaped PANI and PANIS *via* electrochemical oxidation polymerization method, and their electroactivity behaviors

As mentioned previously the star-shaped PANI and PANIS were also synthesized by electrochemical oxidation polymerization method. It is well accepted that, the electrochemical approach is more advantageous since film properties such as conductivity and thickness can be controlled by the electrochemical parameters such as current density, pH, substrate, nature and concentration of electrolyte [9, 11].

The deposition of the star-shaped PANI and PANIS were performed under identified conditions as given in Experimental section (Figure 8a and b). After electropolymerization the effect of the potential scanning rate (V) on the peak currents for the synthesized star-shaped polymers were studied in the range of 10 to 90 mV s^{-1} scan rate, in an aqueous solution of CSA (1.0 mol l^{-1}) (Figure 8c and d). As seen in Figure 8c, the CVs of the star-shaped PANI shows two typical redox couples with anodic peaks at approximately 0.24 and 0.39 V *versus* the Ag/AgCl electrode. In contrast, the star-shaped PANIS (Figure 8d), shows two typical redox couples with anodic peaks at approximately 0.26 and 0.50 V *versus* the Ag/AgCl electrode. Moreover, in both samples the anodic peaks shift in the direction of positive potential with increasing scan rate, which indicates the electrochemical doping/dedoping of the deposited polymer films were chemically reversible.

(Figure 8)

As shown in Figure 9, for additional evidence on the redox stability of the electrochemically synthesized star-shaped PANI and PANIS, the cyclic voltammograms (20 cycles) of the samples were recorded between -0.50 and +1.00 V *versus* Ag/AgCl electrode at a scan rate of 150 mV s⁻¹. As can be seen the S-PANI showed two anodic peaks at approximately 0.47 and 0.71 V *versus* the Ag/AgCl electrode. In similar the S-PANIS also showed two anodic peaks at approximately 0.42 and 0.74 V *versus* the reference electrode. These CVs revealed that the electrochemically synthesized star-shaped PANI and PANIS still retained good redox activity, and the resulting polymers are highly stable.

(Figure 9)

To evaluate the redox activity of the electrochemically synthesized S-PANI, and S-PANIS the effect of the potential scanning rate (V) on the peak currents in the range of 10 to 90 mV s⁻¹ scan rate were determined (Figure 10). This linear relationship is typical of redox active polymers attached to the working electrode (GCE), and also exemplifies the stability of the synthesized samples toward doping/dedoping. In addition, similar to chemically synthesized S-PANI, the electrochemically synthesized S-PANI showed higher electroactivity than those of the S-PANIS. This may be resulted from reducing of conjugated length by methoxy group in the case of the polyanisidine.

(Figure 10)

3.6. UV-visible spectroscopy

The optical properties of the chemically synthesized homo and star-shaped PANI and PANIS were investigated using ultraviolet-visible (UV-vis) spectroscopy. The samples

for UV-vis spectroscopy were prepared by dissolving the same amount of samples in *N*-methylpyrrolidone (NMP) followed by ultrasonic treatment for 15 minutes. The UV-vis spectra of the homo and star-shaped PANI are shown in Figure 11. As seen the UV-vis spectra of both samples were characterized by three electronic transitions. The homo-PANI (H-PANI) shows three electronic transitions at about 326, 457, and 632 nm. The electronic transitions at 326, and 457 nm are related to the overlap of the π - π^* transition of the benzenoid rings of PANI, while the latter is assigned as exciton absorption of the quinoid (quinonimine) rings of PANI. The UV-vis spectrum of the star-shaped PANI (S-PANI) shows three electronic transitions at about 312, 446, and 624 nm. According to the UV-vis spectra the absorption bands of the S-PANI are shifted to shorter wavelength (blue shift) in comparison with homo-PANI.

The UV-vis spectra of the homo and star-shaped PANIS are shown in Figure 12. Similar to S-PANI the star-shaped PANIS (S-PANIS) was characterized by three electronic transitions at about 321, 441, and 627 nm. In contrast, the UV-vis spectrum of the homo-PANIS (H-PANIS) shows four electronic transitions at about 322, 439, 631, and 857 nm [53, 54].

(Figure 11)

(Figure 12)

3.7. Electrospinning of the chemically synthesized star-shaped PANI and PANIS with gelatin

The FE-SEM images of the S-PANI/gelatin (Figure 13a and b), and S-PANIS/gelatin (Figure 13c and d) electrospun nanofibers at different magnifications are shown in Figure

13. As can be seen, these images presented a single phase, which indicated good interactions between the synthesized star-shaped PANI and PANIS with gelatin. The average diameters of these nanofibers are in the size range of 120 ± 30 nm.

(Figure 13)

3.8. Electrical conductivity measurement

The conducting polymers in general and PANI in particular are considered as prospective candidates for electrical and biomedical applications, in part due to their electrical conductivities, and environmental stabilities. The electrical conductivities (σ ; S cm^{-1}) of the synthesized samples were measured by the four-probe technique at room temperature. It is important to note that the experimental determinations were repeated 5 times for each sample to evaluate the sample accuracy. The conductivity was calculated from the following equations:

$$\rho = (V/I) (\pi/\ln 2)d$$

$$\sigma = 1/\rho$$

where V is the voltage, I is the current, d is the thicknesses, and ρ ($\Omega \text{ cm}$) is the volume specific resistivities of the samples. The electrical conductivity results obtained are listed in Table 1. As shown in this table the electrochemically synthesized samples shows higher electrical conductivities than those of the corresponding chemically synthesized polymers.

Moreover, the lower electrical conductivity values of the polyanisidines in comparison with corresponding to polyanilines are originated from the reducing of conjugated length by methoxy group in the case of the polyanisidines.

As expected, in comparison with star-shaped PANI and PANIS, the electrical conductivities of the S-PANI/gelatin, and S-PANIS/gelatin electrospun naofibers would be significantly decreased, since gelatin is not conductive material. Despite, it is well established that the conductivity in the semiconductor range (10^{-5} S cm⁻¹) is sufficient for tissue engineering and other medical regenerative purpose [55, 56]. According to the results obtained from electrical conductivity, and electroactivity studies the conclusion could be drawn that the synthesized star-shaped polymers have higher electrical conductivity, and electroactivity than those of the corresponding homo-polymers. These results originated from the spherical, three-dimensional, and nanostructure morphologies of the star-shaped polymers, which allows sufficient overlapping of π -orbitals.

(Table 1)

3.9. Hydrophilicity and degradation of electrospun naofibers

The surface hydrophilicity of scaffolds could influence the extent of protein adsorption and cell attachment. The surface hydrophilicities of the S-PANI/gelatin, and S-PANIS/gelatin electrospun naofibers were characterized by drop water contact angle at room temperature. It is expected the naofibers possess hydrophilic behavior, in part due to high weight percent of gelatin in the samples (78 wt%). In addition, in the case of our study, the tannic acid core improved the hydrophilicities of the nanofibers. The contact angles of S-PANI/gelatin, and S-PANIS/gelatin electrospun naofibers with water were obtained $76 \pm 2.1^\circ$, and $71 \pm 1.9^\circ$, respectively. In addition, the photographs of water drops

on S-PANI/gelatin (Figure 14a), and S-PANIS/gelatin (Figure 14b) electrospun nanofibers are shown in Figure 14.

(Figure 14)

It should be pointed out that the degradation of tissue engineering scaffolds is beneficial to enable tissue integration, and to avoid subsequent surgical removal of scaffolds. It is expected that the electrospun nanofibers shows good biodegradability, in part due to presence of tannic acid, and high weight percent of gelatin (78 wt%) in the samples. The *in vitro* degradation behaviors of the S-PANI/gelatin, and S-PANIS/gelatin electrospun nanofibers were investigated through evaluating the morphological changes after soaking the nanofibers in phosphate-buffered saline (PBS; Invitrogen, CA, USA) in 37 °C. After 7 days, the specimens were retrieved, and dried with freeze-drying system. The FE-SEM images of the samples are shown in Figure 15. As can be seen in FE-SEM images both S-PANI/gelatin, and S-PANIS/gelatin electrospun nanofibers are undergo to swelling and degradation after 7 days [57, 58].

(Figure 15)

4. Conclusion

Two novel star-shaped conducting polyaniline and polyanisidine *via* a “core-first” method from tannic acid have been successfully synthesized, and characterized. The FE-SEM images exhibited that the synthesized star-shaped polyaniline and polyanisidine have nanostructure, and porous morphologies with an average diameter of 100 ± 20 nm. The electroactivity and electrical conductivity studies showed that the synthesized star-shaped polymers have higher electrical conductivity and electroactivity than those of the corresponding homo-polymers in both chemical and electrochemical approaches. These

results originated from the spherical, three-dimensional, and nanostructured morphologies of the star-shaped polymers, which allows sufficient overlapping of π -orbitals. The FE-SEM images of the S-PANI/gelatin and S-PANIS/gelatin electrospun nanofibers exhibited a single phase, which indicated good interactions between the synthesized star-shaped polymers with gelatin. The average diameters of these nanofibers were in the size range of 120 ± 30 nm. Due to influences of electrical stimulation on the nerve regeneration, we predicted the conductive and biocompatible S-PANI/gelatin and S-PANIS/gelatin electrospun nanofibers can be considered as potential candidates for the fabrication of conductive scaffolds to promote neurite outgrowth and nerve regeneration.

Acknowledgements

We express our gratitude to the Payame Noor University, and Research Center for Pharmaceutical Nanotechnology, Tabriz University of Medical Sciences for supporting this project.

References

- [1] H. Shirakawa, E. J. Louis, A. G. MacDiarmid, C. K. Chiang and A. J. Heeger, *Chem. Commun.*, 1977, 578–580.
- [2] J. Zhong, J. Meng, Z. Yang, P. Poulin and N. Koratkar, *Nano Energ.*, 2015, **17**, 330–338.
- [3] H. Gu, J. Guo, H. Wei, X. Yan, D. Ding, X. Zhang, Q. He, S. Tadakamalla, X. Wang, T. C. Ho, S. Wei and Z. Guo, *J. Mater. Chem. C.*, 2015, **3**, 8152–8165.
- [4] I. Yamaguchi, T. Nagano and L. V. Tuan, *Polymer*, 2015, **73**, 79–85.
- [5] I. A. Ramphal and M. E. Hagerman, *Langmuir*, 2015, **31**, 1505–1515.
- [6] L. Yu, Y. Huang, Z. Wei, Y. Ding, C. Su and Q. Xu, *J. Org. Chem.*, 2015, **80**, 8677–8683.
- [7] M. Jaymand, *Design. Monomer. Polym.*, 2011, **14**, 433–444.
- [8] M. Hatamzadeh, R. Mohammad-Rezaei and M. Jaymand, *Mater. Sci. Semiconduc. Proces.*, 2015, **31**, 463–470.
- [9] M. Jaymand, M. Hatamzadeh and Y. Omid, *Prog. Polym. Sci.*, 2015, **47**, 26–69.
- [10] M. Hatamzadeh, M. Jaymand and B. Massoumi, *Polym. Int.*, 2014, **63**, 402–412.
- [11] M. Jaymand, *Prog. Polym. Sci.*, 2013, **38**, 1287–1306.
- [12] M. Hatamzadeh and M. Jaymand, *RSC Adv.*, 2014, **4**, 28653–28663.
- [13] A. G. Macdiarmid, J. C. Chiang and A. F. Richter, *Synth. Met.*, 1987, **18**, 285–290.
- [14] K. Lee, S. Cho, S. H. Park, A. J. Heeger, C. W. Lee and S.H. Lee, *Nature*, 2006, **441**, 65–68.
- [15] B. Massoumi, M. Hosseinzadeh and M. Jaymand, *J. Mater. Sci. Mater. Electron.*, 2015, **26**, 6057–6067.

- [16] M. Abbasian, M. Jaymand and S. E. S. Bonab, *J. Appl. Polym. Sci.*, 2012, **125**, E131–E140.
- [17] N. Joseph, J. Varghese and M. T. Sebastian, *RSC Adv.*, 2015, **5**, 20459-20466.
- [18] G. Qu, F. Li, E. B. Berda, M. Chi, X. Liu, C. Wang and D. Chao, *Polymer*, 2015, **58**, 60-66.
- [19] J. Wang, X. Han, Y. Ji, H. Ma, *Desalin. Water. Treat.*, 2015, **56**, 356-365.
- [20] B. Massoumi, S. Davtalab, M. Jaymand and A. A. Entezami, *RSC Adv.*, 2015, **5**, 36715–36726.
- [21] G. C. Li, G. R. Li, S. H. Ye and X. P. Gao, *Adv. Energ. Mater.*, 2012, **2**, 1238-1245.
- [22] G. Cai, J. Tu, D. Zhou, J. Zhang, Q. Xiong, X. Zhao, X. Wang and C. Gu, *J. Phys. Chem C.*, 2013, **117**, 15967-15975.
- [23] K. Y. K. Man, H. L. Wong and W. K. Chan, *Langmuir*, 2006, **22**, 3368-3375.
- [24] M. R. Choi, S. H. Woo, T. H. Han, K. G. Lim, S. Y. Min, W. M. Yun, O. K. Kwon, C. E. Park, K. D. Kim, H. K. Shin, M. S. Kim, T. Noh, J. H. Park, K. H. Shin, J. Jang and T. W. Lee, *Chem. Sus. Chem.*, 2011, **4**, 363–368.
- [25] Y. D. Liu, F. F. Fang and H. J. Choi, *Soft. Matter.*, 2011, **7**, 2782–2789.
- [26] R. J. Tseng, J. Huang, J. Ouyang, R. B. Kaner and Y. Yang, *Nano. Let.*, 2005, **5**, 1077-1080.
- [27] J. Huang, S. Virji, B. H. Weiller and R. B. Kaner, *J. Am. Chem. Soc.*, 2003, **125**, 314-315.
- [28] V. R. Devadasu, V. Bhardwaj and M. N. V. R. Kumar, *Chem. Rev.*, 2013, **113**, 1686–1735.

- [29] L. Mei, Z. Zhang, L. Zhao, L. Huang, X. L. Yang, J. Tang and S. S. Feng, *Adv. Drug. Deliv. Rev.*, 2013, **65**, 880-890.
- [30] M. T. M. Pendergast and E. M.V. Hoek, *Energ. Environ. Sci.*, 2011, **4**, 1946–1971.
- [31] A. Mihranyan, N. Ferraz and M. Strømme, *Prog. Mater. Sci.*, 2012, **57**, 875–910.
- [32] Z. L. Wang and W. Wu, *Angew. Chem. Int. Ed.*, 2012, **51**, 11700–11721.
- [33] M. Jaymand, *RSC Adv.*, 2014, **4**, 33935–33954.
- [34] C. L. H. Peng, L. Zhang, G. L. Lu, Y. Wang and J. Travas-Sejdic, *Macromolecules*, 2011, **44**, 6899–6907.
- [35] G. Li and Z. Zhang, *Macromolecules*, 2004, **37**, 2683-2685.
- [36] K. Li, D. Guo, J. Chen, Y. Kong and H. Xue, *Synth. Met.*, 2015, **209**, 555–560.
- [37] B. Massoumi, N. Sorkhi-Shams, M. Jaymand and R. Mohammadi, *RSC Adv.*, 2015, **5**, 21197–21205.
- [38] M. Hassan, K. R. Reddy, E. Haque, S. N. Faisal, S. Ghasemi, A. I. Minett and V. G. Gomes, *Compos. Sci. Technol.*, 2014, **98**, 1–8.
- [39] B. Massoumi, O. Badalkhani, H. Gheybi and A. A. Entezami, *Design. Monomer. Polym.*, 2012, **15**, 357–368.
- [40] Z. J. Gu, Q. C. Zhang and Q. Shen, *J. Polym. Res.*, 2015, **22**, 7.
- [41] Q. Tang, J. Wu, X. Sun, Q. Li, J. Lin and M. Huang, *Chem. Commun.*, 2009, 2166–2167.
- [42] D. Bhattacharjya and I. Mukhopadhyay, *Langmuir*, 2012, **28**, 5893–5899.
- [43] S. Xiong, P. Jia, K. Y. Mya, J. Ma, F. Boey and X. Lu, *Electrochim. Acta.*, 2008, **53**, 3523–3530.
- [44] D. T. Wu, *Synth. Met.*, 2002, **126**, 289–293.

- [45] S. J. T. Rezaei, Y. Bide and M. R. Nabid, *Synth. Met.*, 2011, **161**, 1414–1419.
- [46] N. K. Guimard, N. Gomez and C. E. Schmidt, *Prog. Polym. Sci.*, 2007, **32**, 876–921.
- [47] T. H. Qazi, R. Rai and A. R. Boccaccini, *Biomaterials*, 2014, **35**, 9068-9086.
- [48] A. D. Bendrea, L. Cianga and I. Cianga, *J. Biomater. Appl.*, 2011, **26**, 1–84.
- [49] S. Kamalesh, P. Tan, J. Wang, T. Lee, E. T. Kang and C. H. Wang, *J. Biomed. Mater. A.*, 2000, **52**, 467-478.
- [50] R. Konwarh, S. Pramanik, K. S. P. Devi, N. Saikia, R. Boruah, T. K. Maiti, R. C. Deka and N. Karak, *J. Mater. Chem.*, 2012, **22**, 15062–15070.
- [51] W. Serrano, A. Melendez, I. Ramos, N. J. Pinto, *Polymer*, 2014, **55**, 5727-5733.
- [52] M. Li, Y. Guo, Y. Wei, A. G. MacDiarmid and P. I. Lelkes, *Biomaterials*, 2006, **27**, 2705–2715.
- [53] M. R. Nabid, Z. Zamiraei and R. Sedghi, *Iran. Polym. J.*, 2010, **19**, 699-706.
- [54] B. Wessling, *Polymers*, 2010, **2**, 786-798.
- [55] J. W. Lee, F. Serna, J. Nickels and C. E. Schmidt, *Biomacromolecules*, 2006, **7**, 1692- 1695.
- [56] N. A. Rahman, M. Gizdavic-Nikolaidis, S. Ray, A. J. Easteal and J. Travas-Sejdic, *Synth. Met.*, 2010, **160**, 2015-2022.
- [57] D. Kai, M. P. Prabhakaran, G. Jin and S. Ramakrishna, *J. Biomed. Mater. Res. A.*, 2011, **99**, 376–385.
- [58] Y. Liu, H. Cui, X. Zhuang, Y. Wei and X. Chen, *Acta Biomater.*, 2014, **10**, 5074-5080.

Schemes, Figures, and Table captions:

Scheme 1. Synthesis of phenylamine-functionalized tannic acid macromonomer (PhATAM).

Scheme 2. Synthesis of star-shaped PANI and PANIS *via* chemical oxidation polymerization method.

Figure 1. The FTIR spectra of the tannic acid, and PhATAM.

Figure 2. The ^1H NMR spectra of the tannic acid, and PhATAM.

Figure 3. The FTIR spectra of the star-shaped PANI and homo-PANI.

Figure 4. The FTIR spectra of the star-shaped PANIS and homo-PANIS.

Figure 5. The FE-SEM images of the chemically synthesized homo-PANI (a), homo-PANIS (b), star-shaped PANI (c), and star-shaped PANIS (d).

Figure 6. Cyclic voltammetry curves (CVs) of the chemically synthesized homo-PANI (a), star-shaped PANI (b), homo-PANIS (c), and star-shaped PANIS (d) in the range of 10 to 90 mV s^{-1} scan rate, in the aqueous solution of CSA (1 mol l^{-1}) between -0.20 to +1.00 V.

Figure 7. Linear relationship between current and scan rate in the chemically synthesized homo and star-shaped polymers.

Figure 8. Electrochemically growth of star-shaped PANI (a) and PANIS (b) from PhATAM, and CVs of the electrochemically synthesized star-shaped PANI (c) and PANIS (d) in the range of 10 to 90 mV s^{-1} scan rate, in the aqueous solution of CSA (1 mol l^{-1}) between -0.20 to +1.00 V.

Figure 9. The CVs (20 cycles) of the electrochemically deposited S-PANI and S-PANIS at a scan rate of 150 mV s^{-1} in the aqueous solution of CSA (1 mol l^{-1}) between -0.50 and $+1.00 \text{ V}$.

Figure 10. The effect of the potential scanning rate (V) on the peak currents for the electrochemically synthesized S-PANI, and S-PANIS in the range of 10 to 90 mV s^{-1} scan rate.

Figure 11. The UV-vis spectra of the homo and star-shaped PANI.

Figure 12. The UV-vis spectra of the homo and star-shaped PANIS.

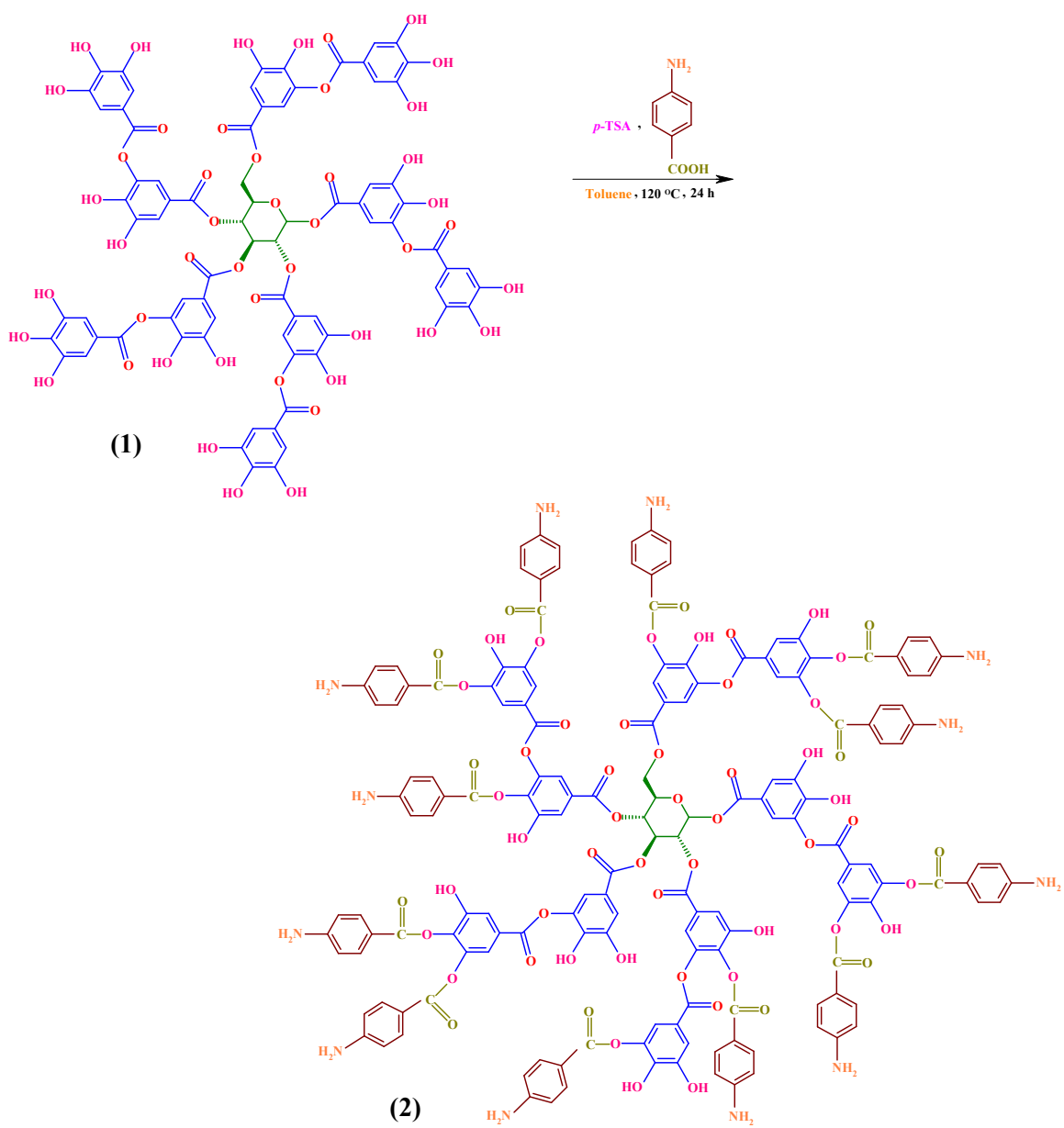
Figure 13. The FE-SEM images of the star-shaped PANI/gelatin (**a** and **b**), and star-shaped PANIS/gelatin (**c** and **d**) electrospun nanofibers at different magnifications.

Table 1. The electrical properties of the synthesized samples.

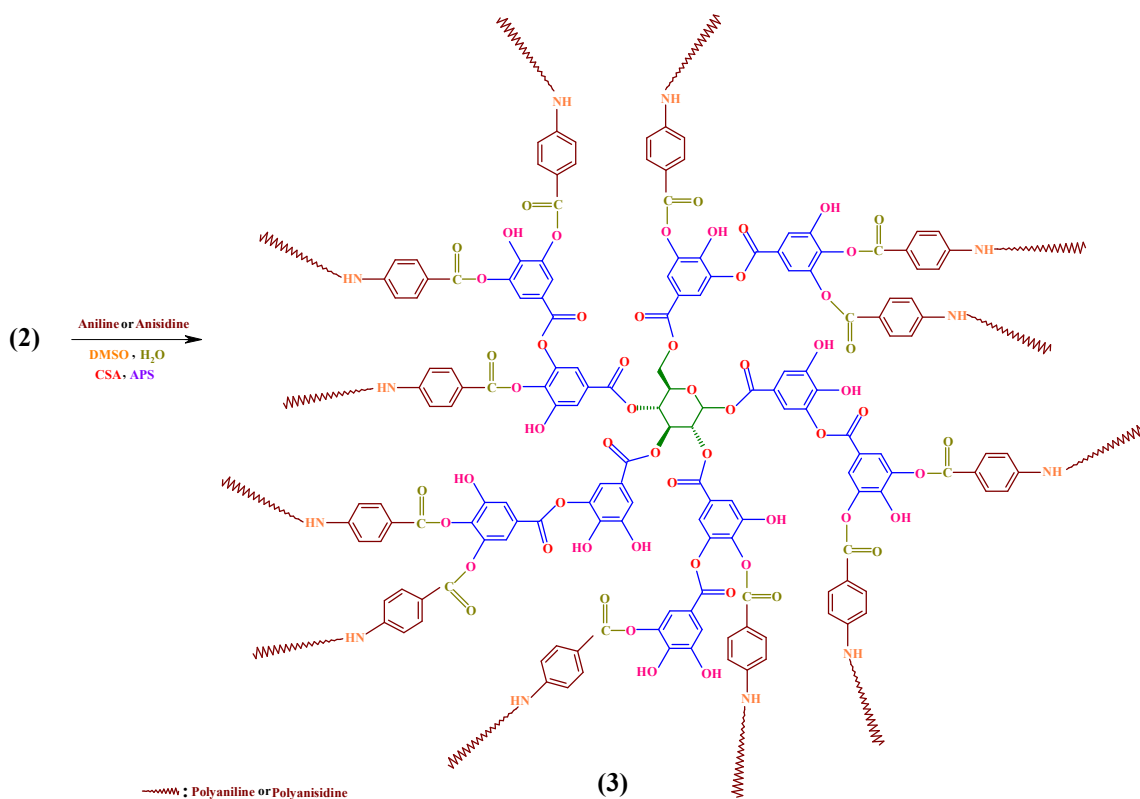
Figure 14. The Photographs of water drops on S-PANI/gelatin (a), and S-PANIS/gelatin (b) electrospun naofibers.

Figure 15. The FE-SEM images of the S-PANI/gelatin (a), and S-PANIS/gelatin (b) electrospun naofibers after 7 days soaking in PBS.

Schemes, Figures, and Table



Scheme 1. Synthesis of phenylamine-functionalized tannic acid macromonomer (PhATAM).



Scheme 2. Synthesis of star-shaped PANI and PANIS *via* chemical oxidation polymerization method.

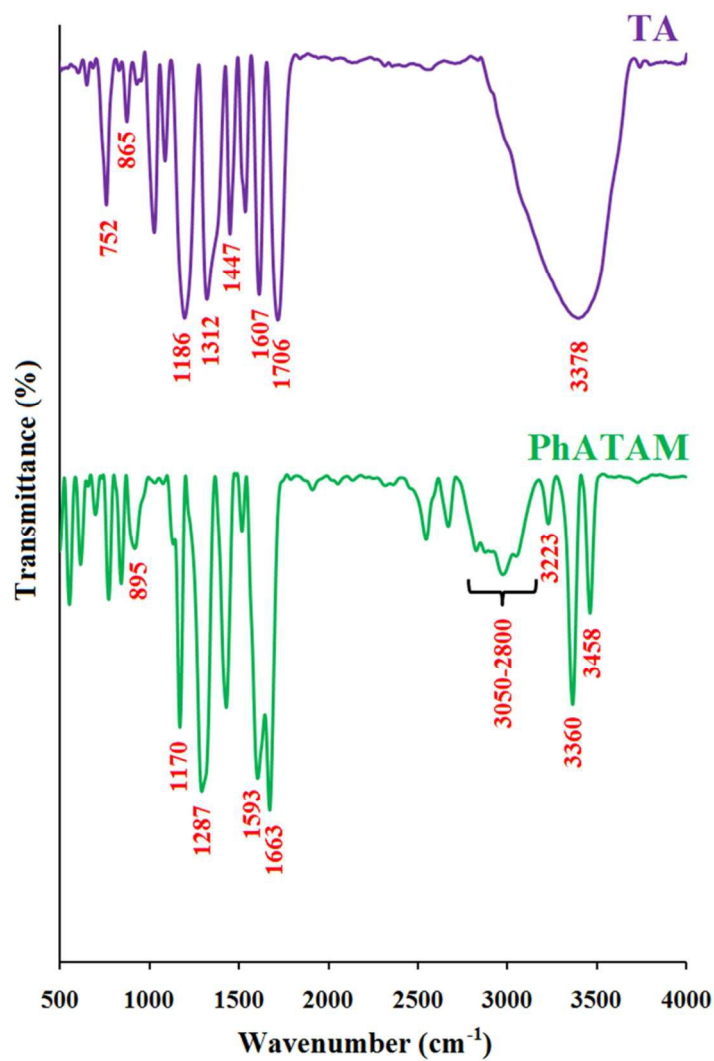


Figure 1. The FTIR spectra of the tannic acid, and PhATAM.

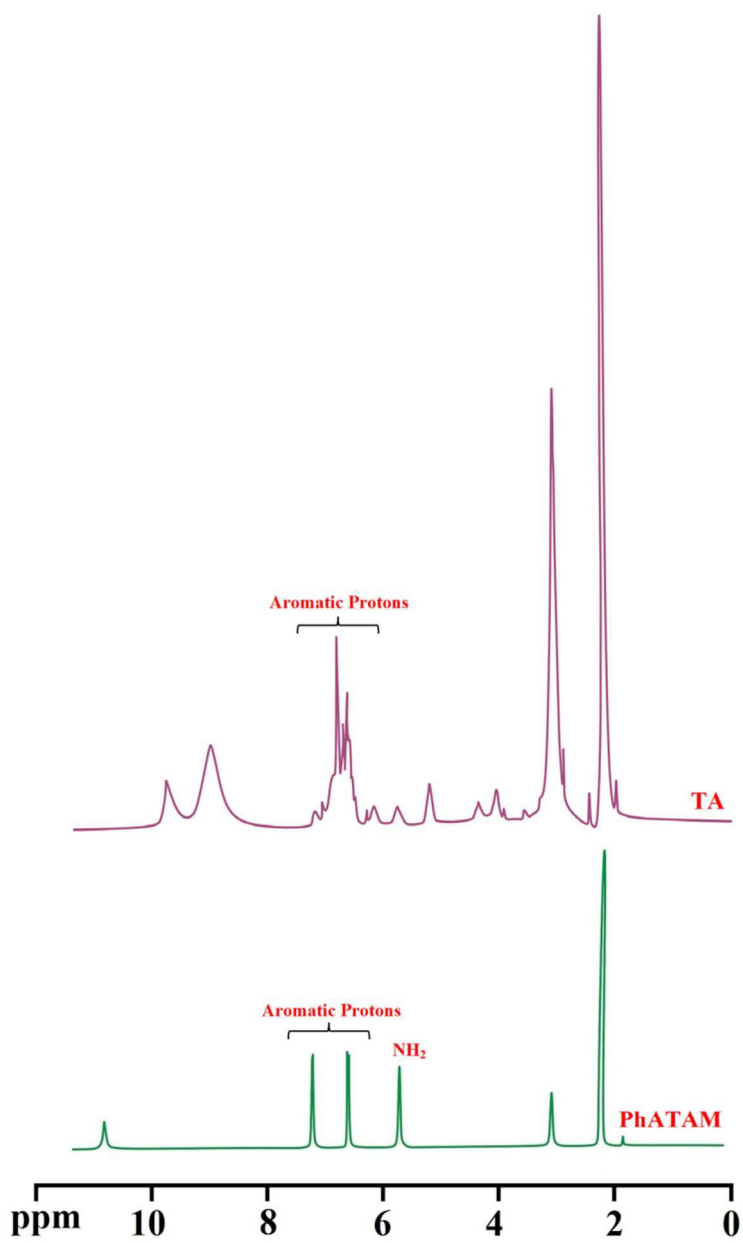


Figure 2. The ^1H NMR spectra of the tannic acid, and PhATAM.

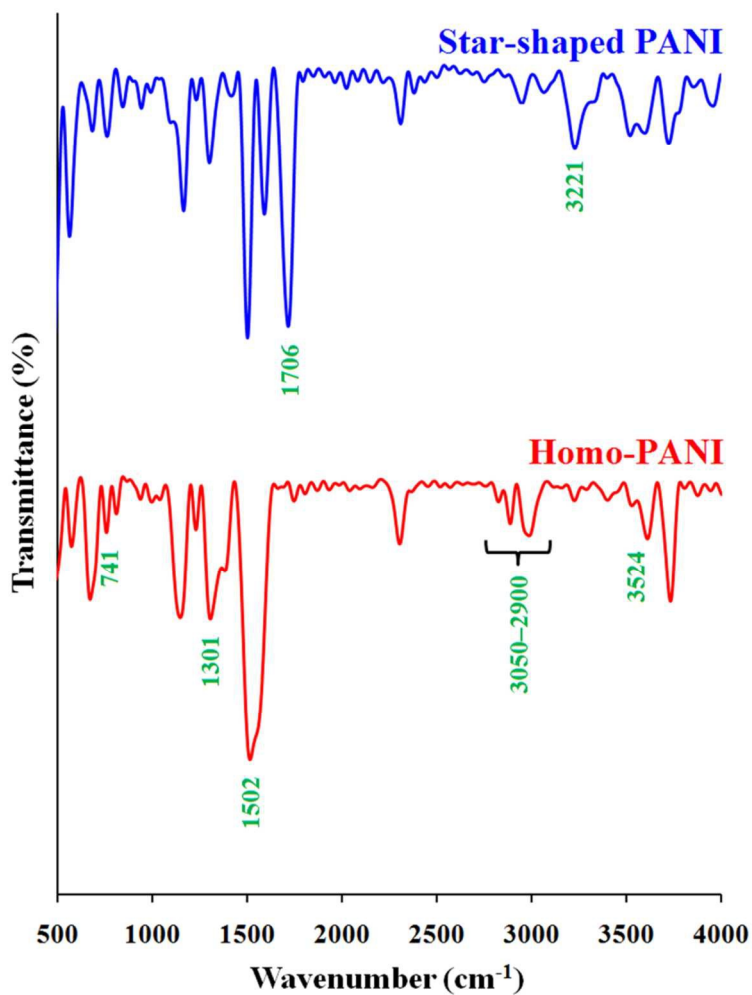


Figure 3. The FTIR spectra of the star-shaped PANI and homo-PANI.

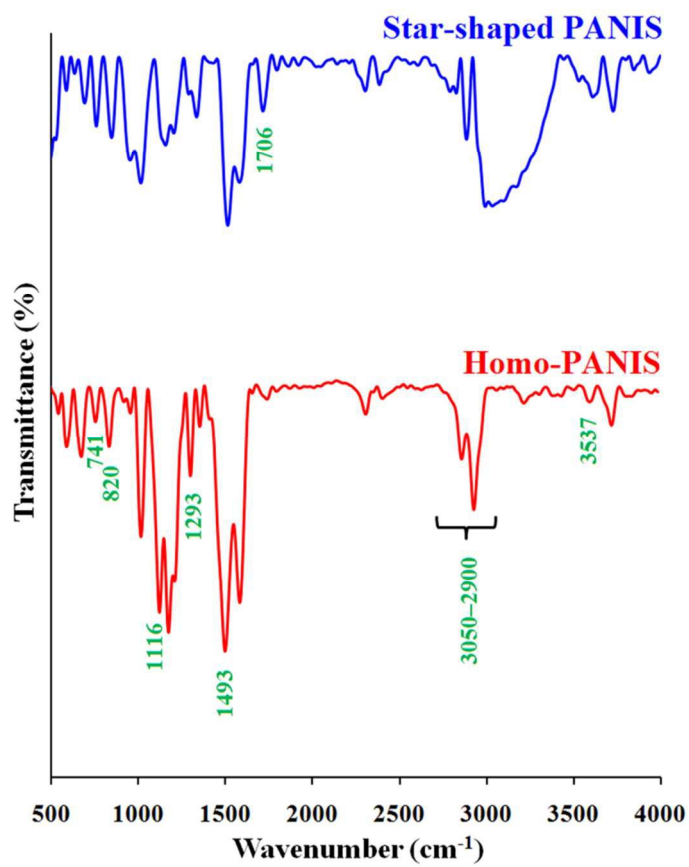


Figure 4. The FTIR spectra of the star-shaped PANIS and homo-PANIS.

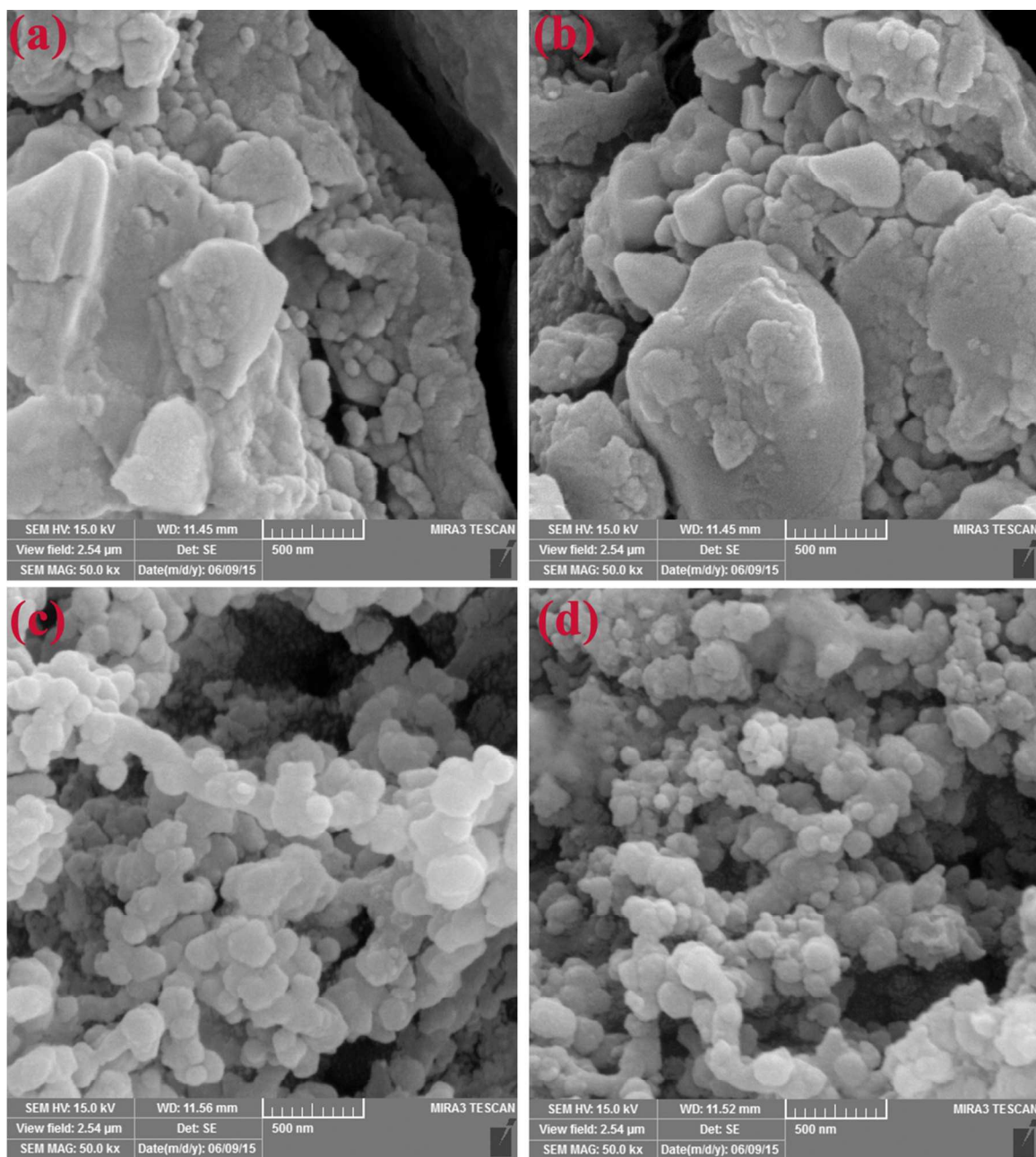


Figure 5. The FE-SEM images of the chemically synthesized homo-PANI (a), homo-PANIS (b), star-shaped PANI (c), and star-shaped PANIS (d).

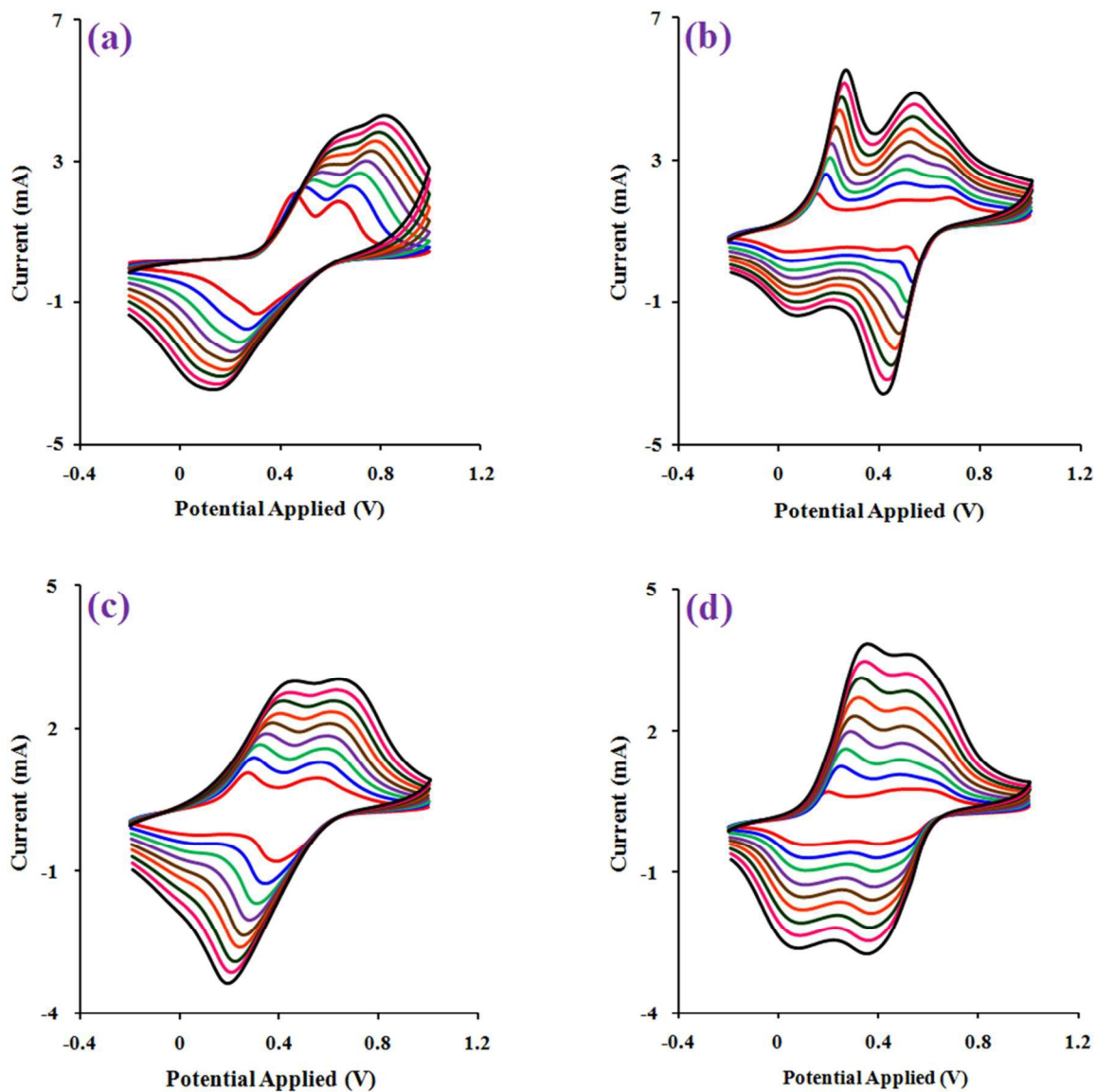


Figure 6. Cyclic voltammetry curves (CVs) of the chemically synthesized homo-PANI (a), star-shaped PANI (b), homo-PANIS (c), and star-shaped PANIS (d) in the range of 10 to 90 mV s^{-1} scan rate, in the aqueous solution of CSA (1 mol l^{-1}) between -0.20 to +1.00 V.

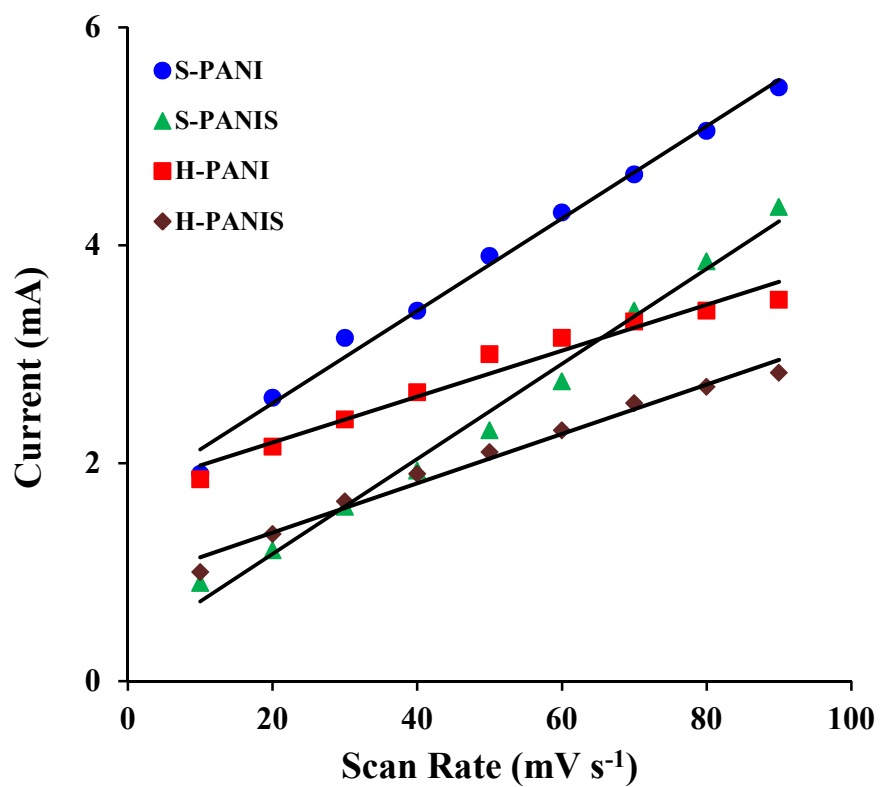


Figure 7. Linear relationship between current and scan rate in the chemically synthesized homo and star-shaped polymers.

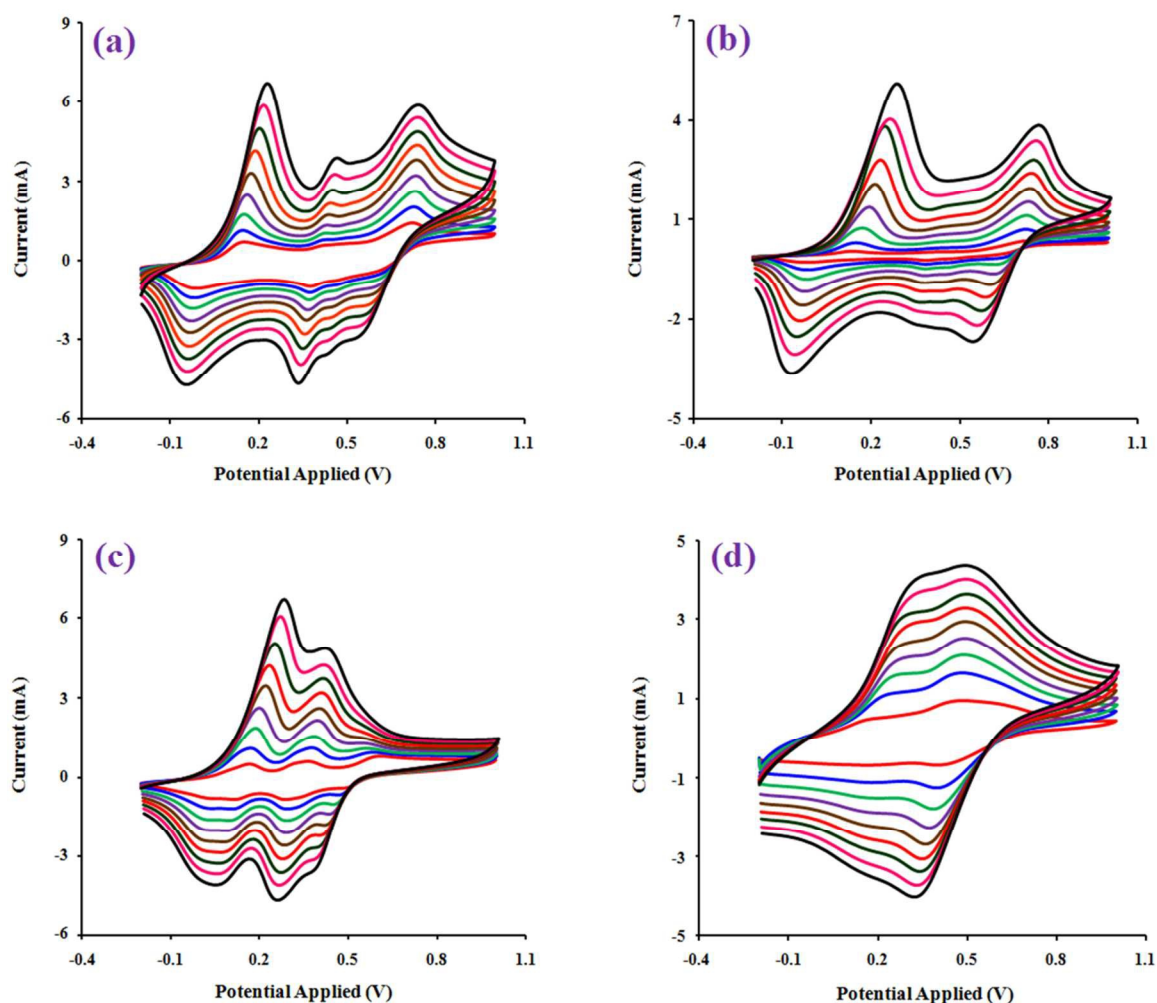


Figure 8. Electrochemically growth of star-shaped PANI (a) and PANIS (b) from PhATAM, and CVs of the electrochemically synthesized star-shaped PANI (c) and PANIS (d) in the range of 10 to 90 mV s^{-1} scan rate, in the aqueous solution of CSA (1 mol l^{-1}) between -0.20 to +1.00 V.

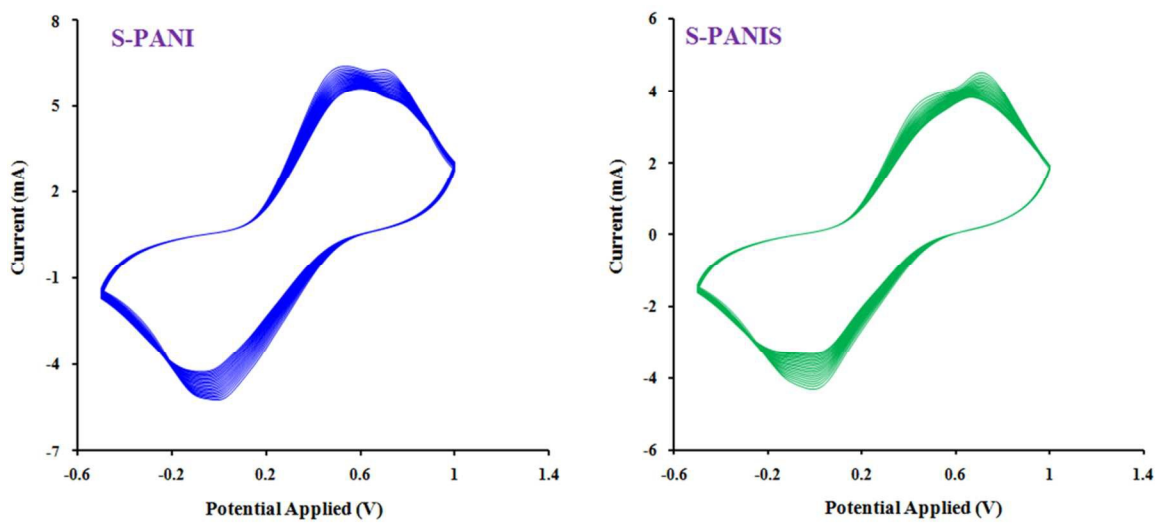


Figure 9. The CVs (20 cycles) of the electrochemically deposited S-PANI and S-PANIS at a scan rate of 150 mV s^{-1} in the aqueous solution of CSA (1 mol l^{-1}) between -0.50 and $+1.00 \text{ V}$.

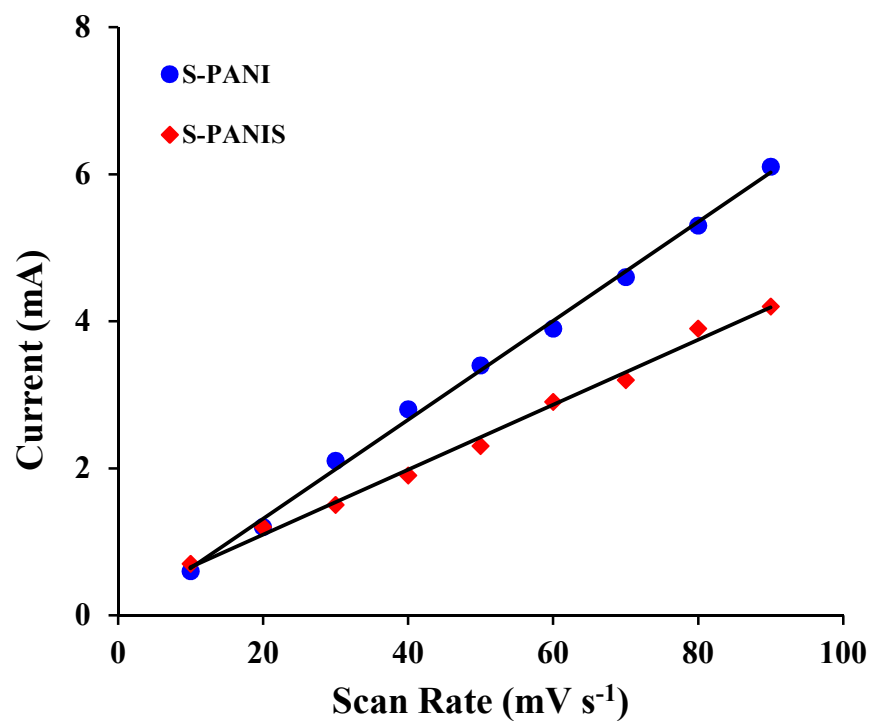


Figure 10. The effect of the potential scanning rate (V) on the peak currents for the electrochemically synthesized S-PANI, and S-PANIS in the range of 10 to 90 mV s⁻¹ scan rate.

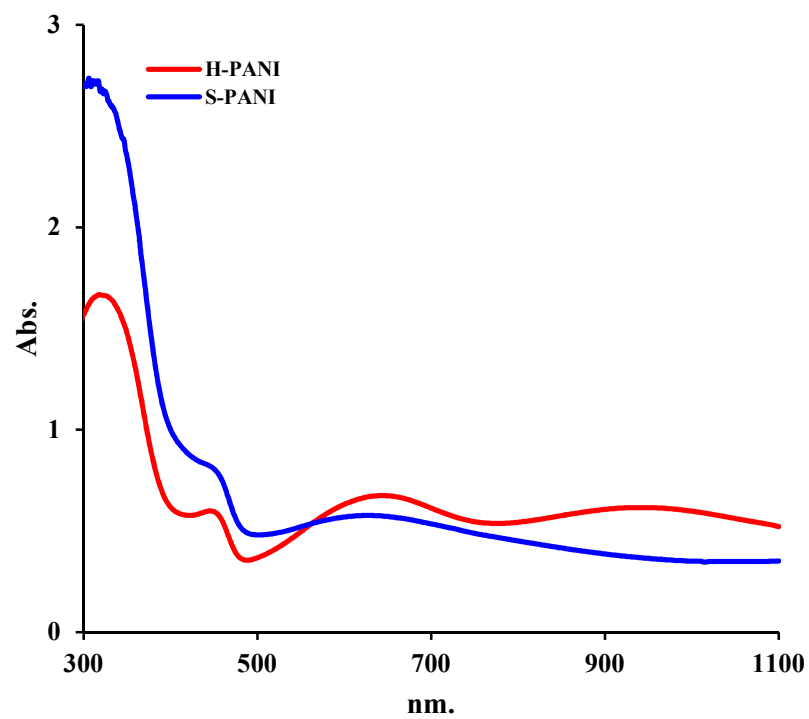


Figure 11. The UV-vis spectra of the homo and star-shaped PANI.

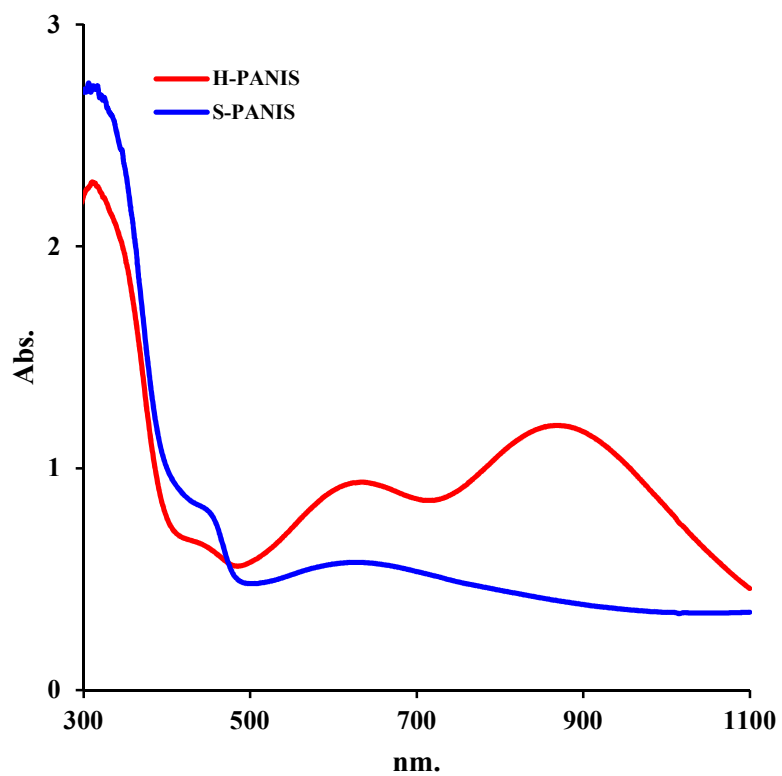


Figure 12. The UV-vis spectra of the homo and star-shaped PANIS.

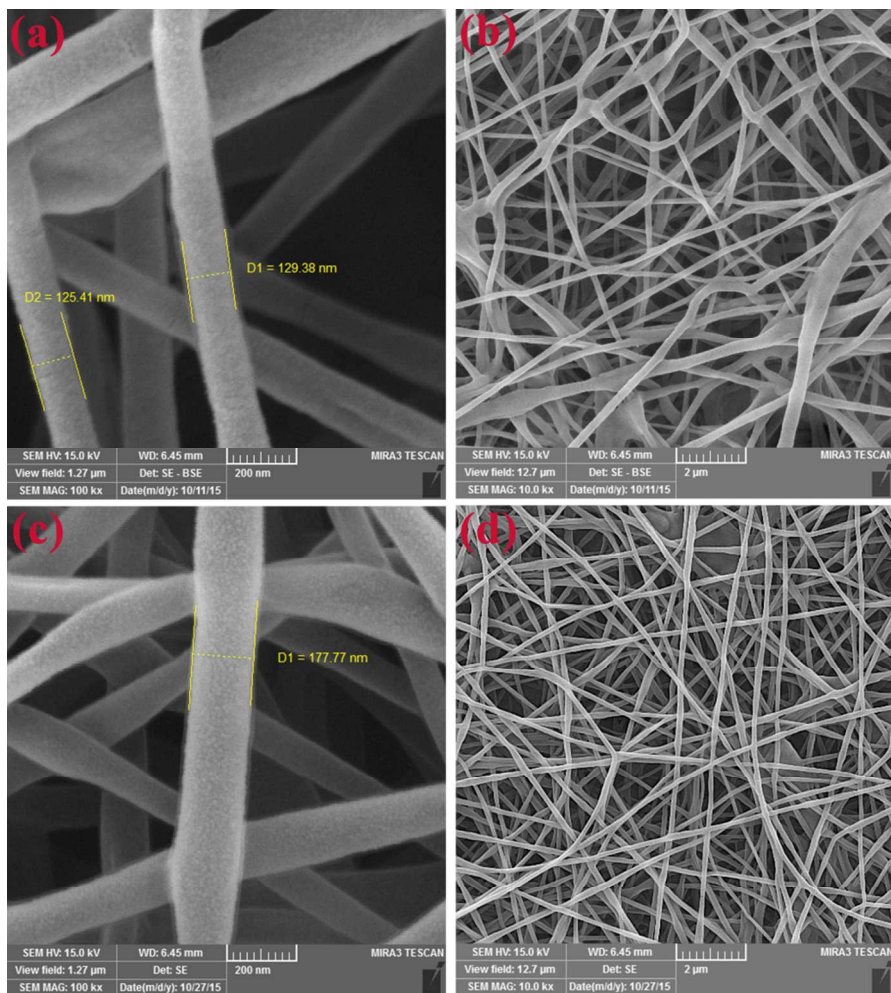


Figure 13. The FE-SEM images of the star-shaped PANI/gelatin (a and b), and star-shaped PANIS/gelatin (c and d) electrospun nanofibers at different magnifications.

Table 1. The electrical properties of the synthesized samples.

Sample	Volume specific resistivity (ρ ; Ω cm)	Electrical conductivity (σ ; S cm ⁻¹)
Chemically synthesized homo-PANI	1.07	0.93
Chemically synthesized homo-PANIS	1.23	0.81
Chemically synthesized star-shaped PANI	0.87	1.14
Chemically synthesized star-shaped PANIS	1.03	0.97
Electrochemically synthesized star-shaped PANI	0.73	1.36
Electrochemically synthesized star-shaped PANIS	0.85	1.17
Star-shaped PANI/gelatin ^a	25	0.04
Star-shaped PANIS/gelatin ^a	33.33	0.03

^a Electrospun nanofibers were provided as given in experimental section.

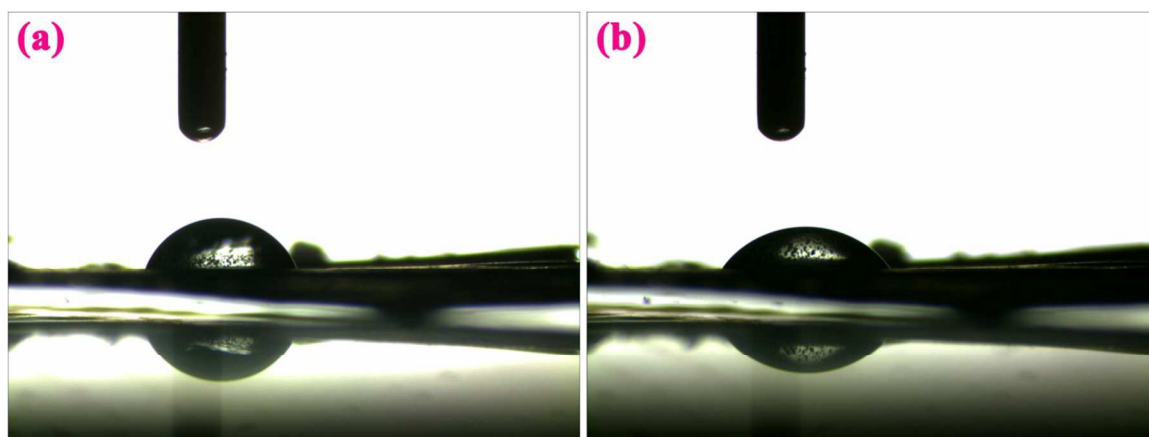


Figure 14. The Photographs of water drops on S-PANI/gelatin (a), and S-PANIS/gelatin (b) electrospun naofibers.

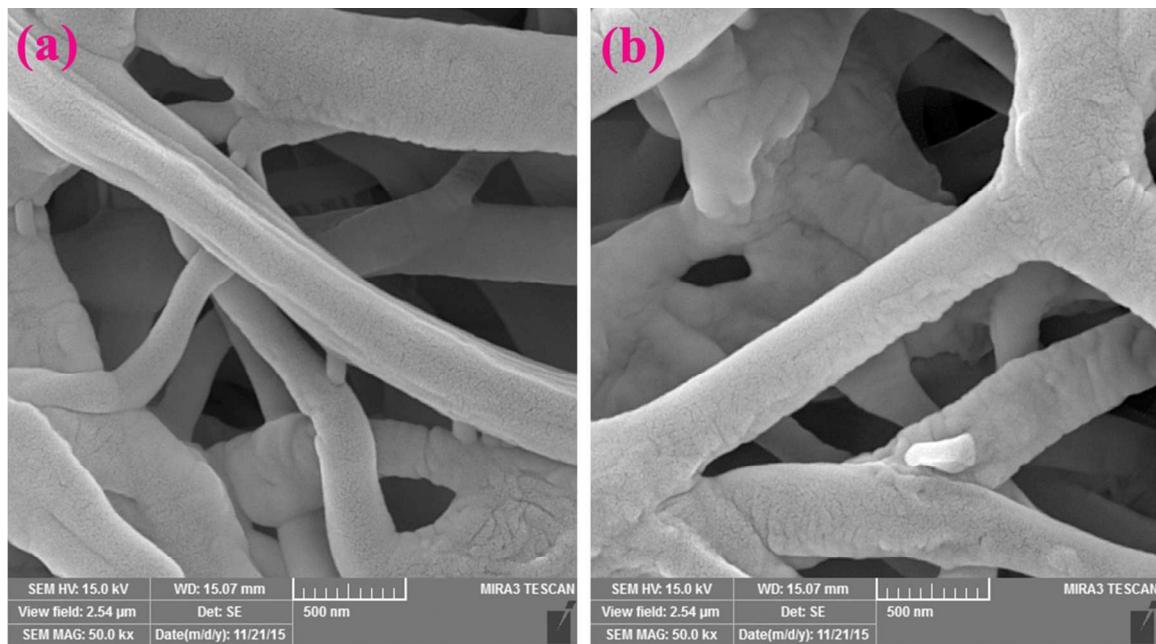
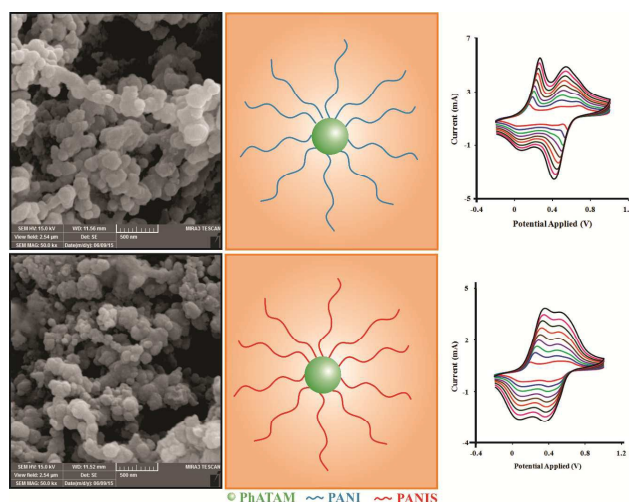


Figure 15. The FE-SEM images of the S-PANI/gelatin (a), and S-PANIS/gelatin (b) electrospun naofibers after 7 days soaking in PBS.

Novel nanostructured star-shaped polyaniline derivatives and their electrospun nanofibers with gelatin

Bakhshali Massoumi¹, Nazila Aali¹, and Mehdi Jaymand^{*,2}

1. Department of Chemistry, Payame Noor University, P.O. BOX: 19395-3697, Tehran, Islamic Republic of Iran.
2. Research Center for Pharmaceutical Nanotechnology, Tabriz University of Medical Sciences, P.O. Box: 51656-65811, Tabriz, Islamic Republic of Iran.



The aim of this study is the synthesis, characterization, and investigation of some physicochemical properties of the star-shaped polyaniline and polyanisidine. In addition, the nanofibers of the synthesized star-shaped polymers with gelatin were also prepared.

* Correspondence to: Mehdi Jaymand, Research Center for Pharmaceutical Nanotechnology, Tabriz University of Medical Sciences, Tabriz, Islamic Republic of Iran.

Tel: +98-41-33367914; Fax: +98-41-33367929

Postal address: Tabriz-5165665811-Iran

E-mail addresses: m_jaymand@yahoo.com; m.jaymand@gmail.com; jaymandm@tbzmed.ac.ir